Direct Sonochemical Preparation and Characterization of Highly Active Mesoporous TiO_2 with a Bicrystalline Framework

Jimmy C. Yu,* Lizhi Zhang, and Jiaguo Yu

Department of Chemistry and Environmental Science Program, The Chinese University of Hong Kong, Shatin, New Territories, Hong Kong

Received April 16, 2002. Revised Manuscript Received August 29, 2002

In this study mesoporous TiO_2 with a bicrystalline (anatase and brookite) framework was synthesized directly under high-intensity ultrasound irradiation. This was carried out separately, both with and without the use of a triblock copolymer. Without thermal treatment, mesoporous TiO_2 was formed by the agglomeration of monodispersed TiO_2 sol particles. The resulting materials were characterized by XRD, TEM, nitrogen adsorption, TGA/DTA, and FTIR. The use of ultrasound irradiation assisted in the formation of the brookite phase. As the content of the brookite phase increased, the pore size and the crystalline sizes of anatase and brookite became larger when the triblock copolymer was used in the synthesis. Both as-prepared samples exhibited better activities than the commercial photocatalyst P25 in the degradation of *n*-pentane in air. The degradation rate of mesoporous TiO_2 synthesized in the presence of triblock copolymer was about two times greater than that of P25. The high activities of the mesoporous TiO_2 with a bicrystalline framework can be attributed to the combined effect of three factors: high brookite content, high surface area, and the existence of mesopores.

Introduction

Mesoporous materials with tailored pore structures and high surface areas have many applications in the areas of adsorption and catalysis.[1] Most studies on the preparation of mesoporous materials appear to be focused on silica because it is more difficult to synthesize mesoporous transition metal oxides, as the inorganic wall is not stable during calcination.[2] In fact, mesoporous transition metal oxides are of particular interest in the synthesis of materials because of their variable oxidation states (properties not possessed by silicates), a capacity which often leads to unusual magnetic, electronic, optical, and catalytic properties.[3,4]

Among the transition metal oxides, TiO_2 is one of the most promising photocatalysts for the treatment of environmental contaminants.[5] After mesoporous TiO_2 with high surface area and narrow pore-size distribution was first synthesized by a modified sol−gel method with phosphorus surfactants as templates by Antonelli and Ying,[6] the preparation of mesoporous TiO_2 has attracted much attention.[7,8] In general, traditional methods for the preparation of mesoporous TiO_2 have many limitations. For example, the mesoporous TiO_2 prepared using traditional phosphate surfactants had low photocatalytic activity because phosphorus from the template was bound so tightly to the mesoporous TiO_2 that it could not be removed completely, by either calcination or solvent extraction.[9] Another problem with traditional methods is that the integrity of the crystalline framework is difficult to maintain under the typical high-temperature thermal/hydrothermal treatment conditions. Furthermore, time-consuming processes such as solvent extraction are often required to remove the surfactants used during the synthesis.[8−10]

Recently, sonochemical processing has been proven to be a useful technique in the synthesis of novel materials with unusual properties.[11,12] Utilizing a sonochemical synthesis method, Wang et al.[13] reported preparation of mesoporous TiO_2 with wormhole-like framework structures by using long-chain amines as the structure-directing agents and titanium isopropoxide as the precursor. They also reported that the selective synthesis of anatase and rutile structure of TiO_2 could be achieved by using titanium isopropoxide and titanium tetrachloride as the precursors, respectively. This synthesis was also carried out via ultrasound irradiation

* Corresponding author. E-mail: jimyu@cuhk.edu.hk. Fax: +852-2603 5057.

(1) Yada, M.; Ohya, M.; Machida, M.; Kijima, T. *Langmuir* **2000**, *16*, 4752.
(2) Elder, S. H.; Gao, Y.; Li, X.; Liu, J.; McCready, D. E.; Windisch, C. F., Jr. *Chem. Mater.* **1998**, *10*, 3140.
(3) Schuth, F. *Chem. Mater.* **2001**, *13*, 3184.
(4) Hu, X.; Antonelli, D. *Angew. Chem., Int. Ed.* **2002**, *41*, 214.
(5) Yu, J. C.; Lin, J.; Kwok, R. W. M. *J. Phys. Chem. B* **1998**, *102*, 5094.
(6) Antonelli, D. M.; Ying, Y. J. *Angew. Chem., Int. Ed. Engl.* **1995**, *34*, 2014.
(7) Kluson, J.; Kacer, P.; Cajthaml, T.; Kalaji, M. *J. Mater. Chem.* **2000**, *11*, 644.
(8) Yang, P.; Zhao, D.; Margolese, D. I.; Chemlka, B. F.; Stucky, G. D. *Chem. Mater.* **1999**, *11*, 2813.
(9) Stone, V. F., Jr.; Davis, R. J. *Chem. Mater.* **1998**, *10*, 1468.
(10) Yue, Y.; Gao, Z. *Chem. Commun.* **2000**, 1755.
(11) Suslick, K. S.; Price, G. J. *Annu. Rev. Mater. Sci.* **1999**, *29*, 295.
(12) Flint, E. B.; Suslick, K. S. *Science* **1991**, *253*, 1397.
(13) Wang, Y.; Tang, X.; Yin, L.; Huang, W.; Hacohen, Y. R.; Gedanken, A. *Adv. Mater.* **2000**, *12*, 1183.

10.1021/cm0203924 CCC: $22.00 © 2002 American Chemical Society
Published on Web 10/09/2002

without the use of any surfactant. Although the resulting materials were mesoporous, their pore-size distributions were quite broad if no further treatment was carried out before and after sonication (hydrolyzed in 0.2 mol/L HCl and precipitated with $NH_3 \cdot H_2O$).[14]

In our previous work,[15] we developed a novel method for the preparation of highly photoactive nanometer-sized TiO_2 photocatalyst with anatase and brookite phases. It was achieved by the hydrolysis of titanium isopropoxide in pure water or a 1:1 $EtOH/H_2O$ solution under ultrasound irradiation using an ordinary ultrasonic cleaning bath, followed by calcination of the samples at 773 K. The photocatalytic activity of the photocatalyst prepared by this method was observed to be higher than that of a commercial photocatalyst (Degussa P25). However, the photocatalytic activity of the uncalcined sample was low because of its poor crystallization.

In this work, we utilized a high-intensity ultrasound probe to directly synthesize mesoporous TiO_2 with a bicrystalline framework of anatase and brookite. The resulting mesoporous TiO_2 has a narrow pore-size distribution. As the content of the brookite phase increased, the pore size and the crystalline sizes of anatase and brookite became larger when a triblock copolymer was used in the synthesis. Mesoporous TiO_2 synthesized either in the absence or presence of a triblock copolymer showed much better activity than the commercial photocatalyst P25. The activities of mesoporous TiO_2 increased even more after calcination.

Experimental Section

Synthesis. Sonochemical preparation of mesoporous TiO_2 with a bicrystalline framework in the presence of triblock copolymer was performed as follows. Typically, 0.032 mol titanium isopropoxide (98%, ACROS) and 3.2 g of triblock copolymer ($EO_{20}PO_{70}EO_{20}$, Aldrich) were dissolved in 20 mL of absolute ethanol. After the mixture was stirred for 1 h, the resulting solution was added to 100 mL of deionized water, drop by drop, under sonication. During the process, the sonication cell was water-cooled to avoid overheating. The suspension was sonicated for 3 h (3 s on, 1 s off, amplitude 95%) by a high-intensity probe (13 mm diameter; Sonics and Materials, VC750, 20 kHz, 100W/cm^2). The powder was collected by centrifugation, washed with deionized water, and dried in an oven at 373 K. The as-prepared sample was calcined at 673 K for 1 h.

Characterization. The low-angle and wide-angle powder X-ray diffraction (XRD) patterns were recorded on a Rigaku D/MAX-RB diffractometer and a Philips MPD 18801 diffractometer using CuKα irradiation, respectively.

Transmission electron microscopy (TEM) study was carried out on a Philips CM-120 electron microscopy instrument. The samples for TEM were prepared by dispersing the final powders in ethanol; the dispersion was then dropped on carbon−copper grids.

The nitrogen adsorption and desorption isotherms at 77 K were measured using a Micrometritics ASAP2010 system after samples were vacuum-dried at 473 K overnight.

Thermalgravimetric analysis (TGA) and differential thermal analysis (DTA) were performed using a Netzsch STA 409C thermal analyzer under air flow of 100 mL/min with a heating rate of 10 K/min from room temperature to 773 K.

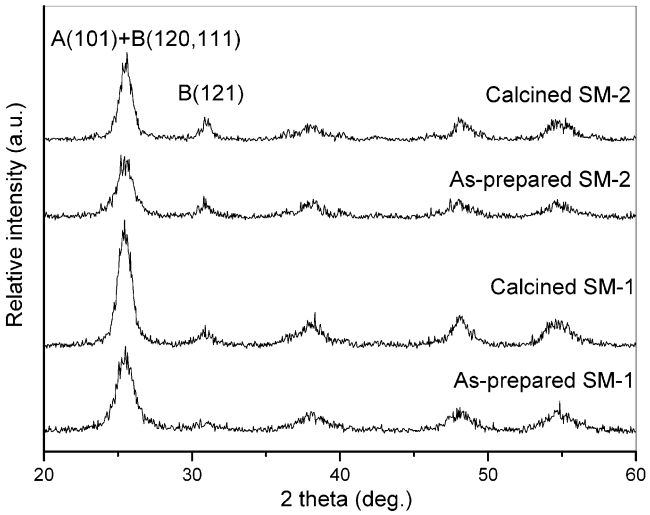

Figure 1. Wide-angle XRD patterns of the as-prepared and calcined SM-1 and SM-2: A denotes anatase, B denotes brookite.

Infrared (IR) spectra on pellets of the samples mixed with KBr were recorded on a Nicolet Magna 560 FTIR spectrometer at a resolution of 4 cm^{-1}. The concentration of the samples was kept around 0.25−0.3%.

A Varian Cary 100 Scan UV−visible system equipped with a labsphere diffuse reflectance accessory was used to obtain the reflectance spectra of the catalysts over a range of 200−600 nm. Labsphere USRS-99-010 was employed as a reflectance standard.

Measurement of Photocatalytic Activity. The photocatalytic activity experiments on the mesoporous TiO_2 for the oxidation of *n*-pentane in air were performed at ambient temperature using a 3000-mL reactor. The photocatalysts were prepared by coating an aqueous suspension of mesoporous TiO_2 onto three dishes with a diameter of 5.0 cm. The weight of the photocatalyst used for each experiment was kept at 0.30 g. The dishes containing the photocatalyst were pretreated in an oven at 100 °C for 1 h and then cooled to room temperature before use.

After the dishes coated with the photocatalysts were placed in the reactor, a small amount of *n*-pentane was injected into the reactor with a syringe. The reactor was connected to a pump and a dryer containing $CaCl_2$ to adjust the starting concentration of *n*-pentane and control the initial humidity in the reactor. The analysis of *n*-pentane, carbon dioxide, and water vapor concentration in the reactor was performed with a Photoacoustic IR multi-gas monitor (INNOVA Air Tech Instruments model 1312). The *n*-pentane vapor was allowed to reach adsorption equilibrium with the photocatalyst in the reactor prior to experimentation. The initial concentration of *n*-pentane after the adsorption equilibrium was 400 ppm, which remained constant until a 15-W 365-nm UV lamp (Cole-Parmer Instrument Co.) in the reactor was turned on. The initial concentration of water vapor was 1.20 ± 0.01 vol % and the initial temperature was 25 ± 1 °C.

Results and Discussion

Formation of Bicrystalline Phase and the Effects of Triblock Copolymer. To characterize the crystalline structure of the samples synthesized either in the absence or presence of triblock copolymer, their XRD patterns (Figure 1) were obtained. All patterns show the presence of anatase (JCPDS, no. 21-1272) and brookite (JCPDS, no. 29-1360). According to Zhang and Banfield,[16] the phase content of a sample can be cal-

(14) Huang, W.; Tang, X.; Wang, Y.; Koltypin, Y.; Gedanken, A. *Chem. Commun.* **2000**, 1415.

(15) Yu, J. C.; Yu, J. G.; Ho, W. K.; Zhang, L. Z. *Chem. Commun.* **2001**, 1942.

(16) Zhang, H.; Banfield, J. F. *J. Phys. Chem. B* **2000**, *104*, 3481.

Table 1. Summary of the Physicochemical Properties of the As-Prepared and Calcined SM-1, SM-2, and P25

	anatase		brookite				
material	crystalline size[a] (nm)	content (%)[b]	crystalline size[a] (nm)	content (%)[b]	S_{BET}[c] (m^2/g)	pore size[d] (nm)	pore volume[e] (cm^{-3}/g)
as-prepared SM-1	6.2	55.5	3.0	44.5	172	6.0	0.27
calcined SM-1	7.7	59.5	5.4	40.5	112	6.7	0.24
as-prepared SM-2	6.9	49.5	9.1	50.5	192	7.3	0.32
calcined SM-2	7.5	51.0	11.5	49.0	128	9.2	0.30
P25	37	80	90[f]	20[g]	55		0.12

[a] Calculated by the Scherrer formula. [b] Calculated using the formula in ref 14. [c] BET surface area calculated from the linear part of the BET plot. [d] Estimated using the adsorption branch of the isotherm. [e] Single point total pore volume of pores at $P/P_0 = 0.97$. [f] The crystalline size of rutile as calculated by the Scherrer formula. [g] The content of rutile.

culated from the integrated intensities of anatase(101), rutile(110) and brookite(121) peaks with the following formulas:

$$W_A = \frac{k_A A_A}{k_A A_A + A_R + k_B A_B} \quad (1)$$

$$W_R = \frac{A_R}{k_A A_A + A_R + k_B A_B} \quad (2)$$

$$W_B = \frac{k_B A_B}{k_A A_A + A_R + k_B A_B} \quad (3)$$

In eq 1, 2, and 3, W_A, W_R, and W_B represent the weight fractions of anatase, rutile, and brookite, respectively. The other symbols A_A, A_R, and A_B are the integrated intensities of anatase(101), rutile(110), and brookite(121) peaks, respectively. The variables k_A and k_B are two coefficients. It was found that $k_A = 0.886$ and $k_B = 2.721$.[16] The calculated phase contents of anatase and brookite are shown in Table 1.

The structure of anatase has been described in terms of chains of distorted TiO_6 octahedra having common edges,[17] whereas brookite is formed by joining together the distorted TiO_6 octahedra sharing three edges.[18] However, the formation mechanism of brookite is not well understood. Usually, tedious hydrothermal treatment in the presence of a strong acid or base is necessary for its synthesis.[19,20] It is also known that the alkali ions play an important role for nucleation of the brookite phase.[21] However, in our study, the synthesis was performed at a neutral pH and in the absence of alkali ions. It can therefore be seen that the unique conditions of ultrasound irradiation can assist the formation of the more distorted TiO_6 octahedron in brookite.

In our previous work,[15] TiO_2 particles containing 80% anatase and 20% brookite were prepared under sonication in an ordinary ultrasound cleaning bath. However, with an increase in the amount of ethanol (with the mole ratio of ethanol to water being 1), the intensities of anatase peaks became steadily weaker and those of the brookite phase disappeared. In this study utilizing a powerful ultrasound probe, the content of brookite increased up to 44.5% even in the mixture of water and ethanol. During the synthesis, the formation of brookite is believed to be temperature dependent. When the sonication of titanium isopropoxide in water was carried out without cooling under high-intensity ultrasound irradiation, only anatase was formed. In contrast, a mixture of brookite and anatase with particle size of 2.5 nm was produced with cooling.[14]

Table 1 shows a summary of the crystalline sizes calculated by the Scherrer formula. The crystalline sizes of anatase and brookite synthesized in the absence of a triblock copolymer (SM-1) are smaller than those synthesized in the presence of the triblock copolymer (SM-2). Table 1 also shows that the brookite content increases when a triblock copolymer is used during the synthesis. It seems that the hybrid inorganic/organic precursor formed between the triblock copolymer and titanium isopropoxide may promote the formation of the brookite phase. H. Kominami et al.[21] also reported that surfactants such as sodium laurate could enhance the nucleation of brookite because a mixture of anatase and rutile phase was formed in the absence of sodium laurate.

After calcination, both anatase and brookite in SM-1 and SM-2 grew larger. More brookite in SM-1 was transformed into anatase than in SM-2 during the calcination. This could be due to the different crystalline sizes of brookite. Zhang and Banfield[16] found that when crystalline sizes were less than 11 nm, anatase was the most stable phase; whereas when crystalline sizes were between 11 and 35 nm, brookite was the most stable phase. Because the crystalline sizes of brookite in both as-prepared SM-1 and SM-2 are less than 11 nm, it could have been transformed into anatase during calcination. However, the crystalline size of brookite in the as-prepared SM-2 was larger than that in SM-1, so less brookite was transformed into anatase in the as-prepared SM-2.

Formation of Mesopores under High-Intensity Ultrasound Irradiation. Figures 2 and 3 respectively show the N_2 adsorption−desorption isotherms and pore-size distribution (BJH) of the as-prepared SM-1 and SM-2. Both isotherms of the samples are type IV with H2 hysteresis-loop, characteristic of mesoporous materials.[22] The pore-size distributions of SM-1 and SM-2 are quite narrow. The BET surface areas (S_{BET}), average pore diameter, and pore volumes of all materials are given in Table 1.

(17) Croner, D. T.; Herrington, K. *J. Am. Chem. Soc.* **1955**, *77*, 4708.
(18) Baur, V. W. H. *Acta Crystallogr.* **1961**, *14*, 214.
(19) Nagase, T.; Ebina, T.; Iwasaki, T.; Hayashi, H.; Onodera, Y.; Chatterjee, M. *Chem. Lett.* **1999**, 911.
(20) Pottier, A.; Chaneac, C.; Tronc, E.; Mazerolles, L.; Jolivet, J. P. *J. Mater. Chem.* **2001**, *11*, 1116.
(21) Kominami, H.; Kohno, M.; Kera, Y. *J. Mater. Chem.* **2000**, *10*, 1151.
(22) Sing, K. S. W.; Evertt, D. H.; Haul, R. A. W.; Moscou, L.; Pierotti, R. A.; Rouquerol, J.; Siemieniewska, T. *Pure Appl. Chem.* **1985**, *57*, 603.

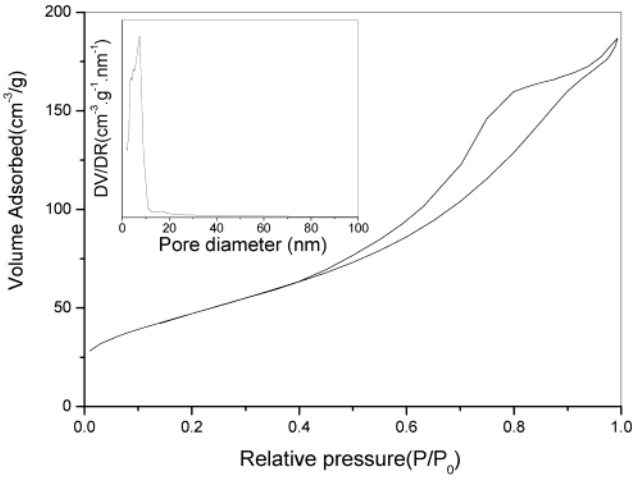

Figure 2. N_2 adsorption−desorption isotherms and BJH pore-size distribution plot (inset) of the as-prepared SM-1.

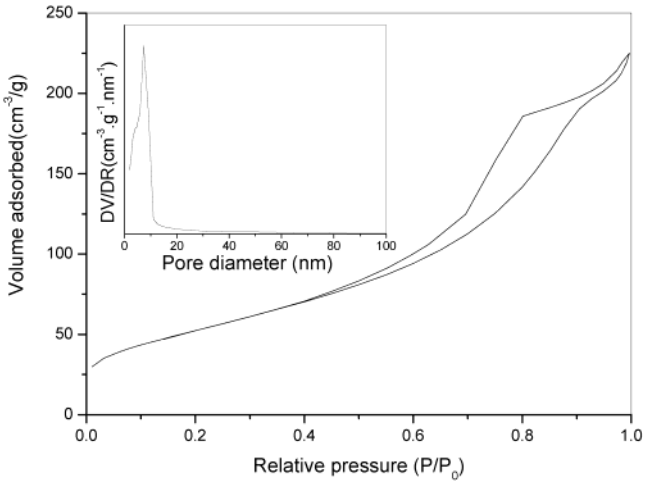

Figure 3. N_2 adsorption−desorption isotherms and BJH pore-size distribution plot (inset) of the as-prepared SM-2.

We believe that the mesoporous structure of SM-1 was formed by the agglomeration of TiO_2 sol nanoparticles under high-intensity ultrasound irradiation. Slow hydrolysis under high-intensity ultrasound irradiation promotes the formation of monodispersed TiO_2 sol particles. Thus, the mesoporous TiO_2 with relatively narrow pore-size distribution was produced by the ultrasound-induced agglomeration of monodispersed TiO_2 sol particles.[23]

The agglomeration of monodispersed TiO_2 particles can be clearly observed in the TEM image (Figure 4A). Figure 4 shows the TEM images of the as-prepared SM-1 and SM-2. It shows that both SM-1 and SM-2 have wormhole-like pore structures, which are connected randomly and lack discernible long-range order in the pore arrangement among the small TiO_2 particles. These small particles are several nanometers in size. Similar disordered channel systems have also been observed for disordered mesoporous silicas and aluminas.[24−26] Figure 5 shows the low-angle XRD patterns of the as-prepared SM-1 and SM-2. The single broad XRD peak of the as-prepared SM-1 in the low angle

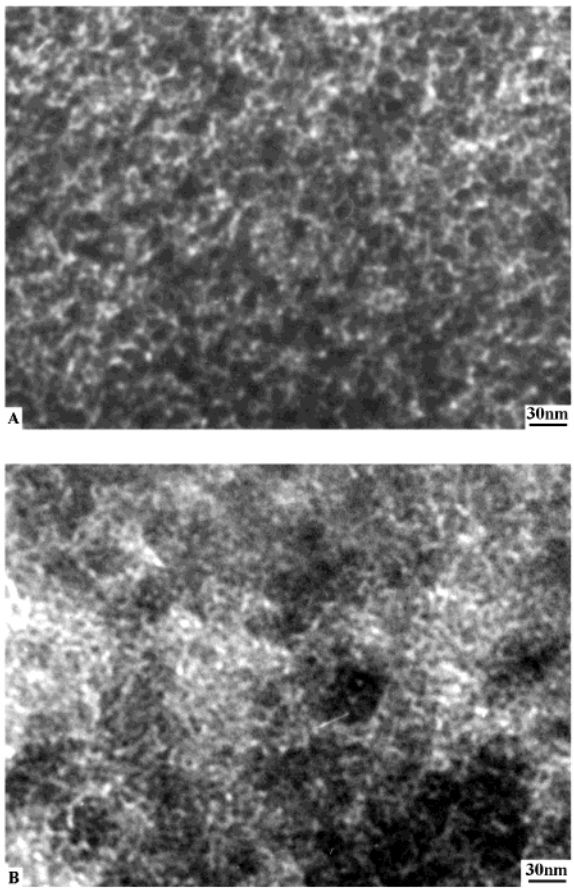

Figure 4. TEM images of the as-prepared SM-1(A) and SM-2(B).

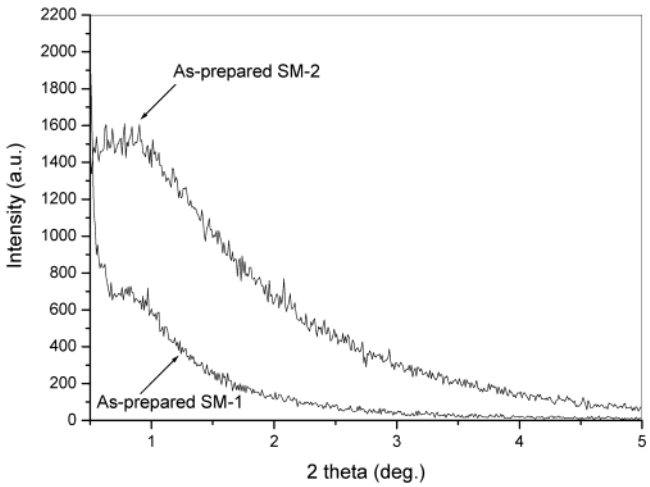

Figure 5. Low-angle XRD patterns of the as-prepared SM-1 and SM-2.

range also indicates that no discernible long-range order in the pore arrangement exists in the as-prepared SM-1, consistent with the TEM image.

The TEM image (Figure 4B) and low-angle XRD pattern (Figure 5) of the as-prepared SM-2 show that the mesoporous structure of SM-2 is also disordered.

(23) Yu, J. C.; Zhang, L. Z.; Yu, J. G. *New J. Chem.* **2002**, *26*, 416.
(24) Tanev, P. T.; Pinnavaia, T. J. *Science* **1995**, *267*, 865. Brashaw, S. A.; Prouzet, E.; Pinnavia, T. J. *Science* **1995**, *269*, 1242. Brashaw, S. A.; Pinnavia, T. J. *Angew. Chem., Int. Ed. Engl.* **1996**, *35*, 1102.
(25) Wen, Y.; Jin, D.; Ding, T.; Shih, W.; Liu, X.; Cheng, S. Z. D.; Fu, Q. *Adv. Mater.* **1998**, *3*, 313. Pang, J. B.; Qiu, K. Y.; Wei, Y.; Lei, X. J.; Liu, Z. F. *Chem. Commun.* **2000**, 477. Pang, J. B.; Qiu, K. Y.; Wei, Y. *J. Non-Crystal. Solids* **2001**, *283*, 101.
(26) Jansen, J. C.; Shan, Z.; Marchese, L.; Zhou, W.; Puil, N. V. D.; Maschmeyer, Th. *Chem. Commun.* **2001**, 713.

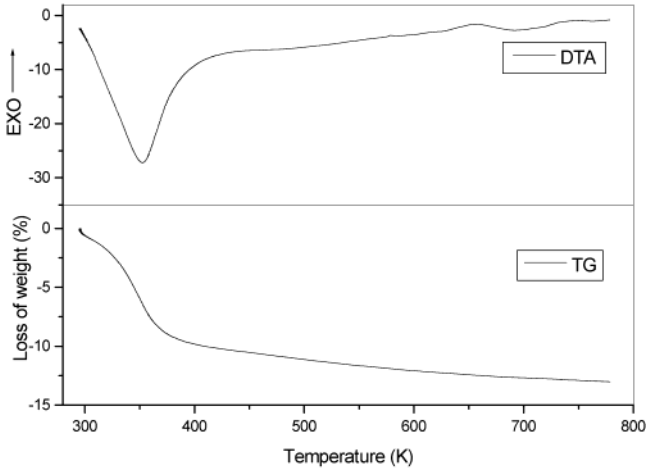

Figure 6. TGA/DTA curves of the as-prepared SM-1.

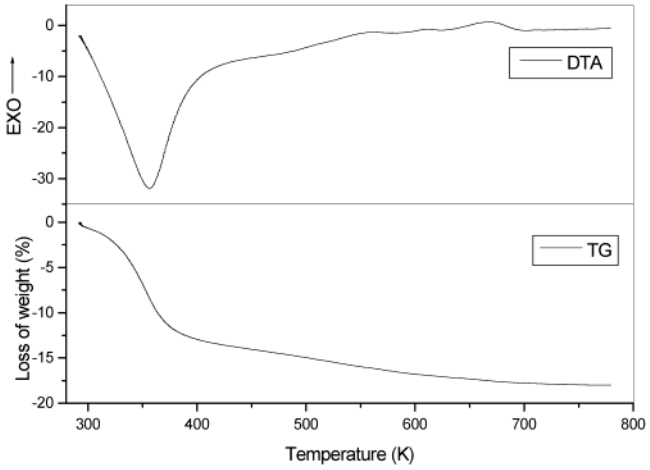

Figure 7. TGA/DTA curves of the as-prepared SM-2.

The formation of such disordered structure can be explained by a series of chemical and physical interactions. At first a hybrid mesostructured inorganic/organic precursor is formed by the assembly of triblock copolymer and titanium isopropoxide through N^0I^0 pathway. Then the high-intensity ultrasound irradiation destroys the ordered mesostructure during the hydrolysis of this inorganic/organic precursor, as the interaction within the precursor is through weak hydrogen bonding. Finally, the mesoporous structure of SM-2 is obtained by the agglomeration of monodispersed TiO_2 sol particles. Although the use of the triblock copolymer does not result in ordered mesoporous TiO_2, it enhances the crystalline size and the pore size of SM-2 (Table 1).

TGA/DTA Studies. The TGA/DTA curves of the as-prepared SM-1 and SM-2 are presented in Figures 6 and 7, respectively. Of the two observed weight losses, the first one corresponds to the removal of ethanol and adsorbed water, measuring to about 10% and 14% for the as-prepared SM-1 and SM-2, respectively. This weight loss corresponds to a larger endothermic peak at about 350 K. The extent of the second weight losses of SM-1 and SM-2 in the range of 473−673 K are almost the same (about 4%), corresponding to the condensation of the hydroxyl groups linked to titanium.[27] The weak

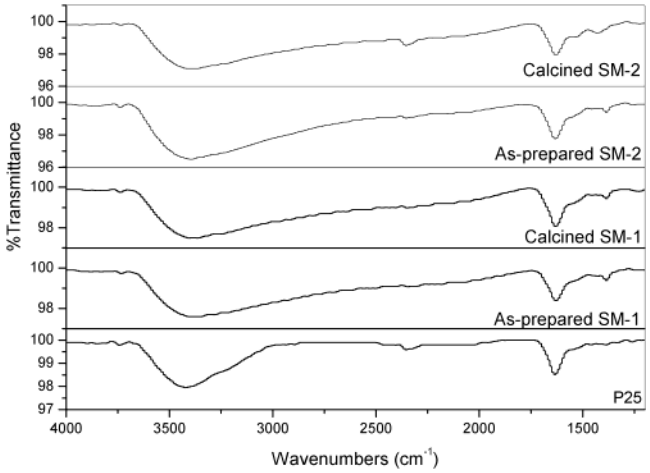

Figure 8. FTIR spectra of the as-prepared and calcined SM-1, SM-2, and P25.

exothermic peaks at around 663 K appearing in both DTA curves are attributed to the crystallization of small amounts of amorphous TiO_2 in the as-prepared SM-1 and SM-2. We attributed the other weak exothermic peak at around 723 K in the DTA curve of the as-prepared SM-1 to the phase transformation of brookite to anatase. This can explain why the content of brookite decreases after thermal treatment. Because this peak cannot be observed in the DTA curve of SM-2, it can be deduced that the content of brookite of SM-2 did not change significantly after calcination. The total weight loss of SM-2 is 18%. This is significantly lower than the 53% loss in the sonochemical preparation of mesoporous TiO_2 using octadecylamine as the structure-directing agent.[27] One possible explanation is that, unlike the interaction of the triblock copolymer and titanium isopropoxide, the interaction between octadecylamine and titanium isopropoxide is strong enough that even octadecylamine cannot be removed with the aid of high-intensity ultrasound irradiation. Although the surface area of more than 800 m^2/g for the mesoporous TiO_2 sonochemically prepared by using octadecylamine as the structure-directing agent is four times larger than that of SM-2, the as-prepared and extracted samples were amorphous. Amorphous TiO_2 is not photoactive, and therefore not useful for photocatalysis. To obtain the anatase phase, calcination at 723 K for 4 h was necessary. However, the thermal treatment reduced the surface area to a mere 79 m^2/g,[13] much lower than that of the as-prepared SM-2 containing anatase and brookite phases.

FTIR Spectra. Figure 8 shows the FTIR spectra of the as-prepared and calcined SM-1, SM-2, and the commercial photocatalyst P25. The two peaks at 3400 and 1650 cm^{-1} correspond to the surface adsorbed water and the hydroxyl groups.[28] No peak corresponding to C−C bonds can be observed on the FTIR spectra of the as-prepared SM-2. This demonstrates that ultrasound irradiation not only accelerates the crystallization process of titania, but also enhances the extraction of triblock copolymer from the hybrid inorganic/organic precursor. Therefore, the hydrolysis of titanium isopropoxide, crystallization of amorphous TiO_2, and extrac-

(27) Wang, Y. Q.; Chen, S. G.; Tang, X. H.; Palchik, O.; Koltypin, Y.;. Gedanken, A. *J. Mater. Chem.* **2001**, *11*, 521.

(28) Ding, Z. G.; Lu, Q.; Greenfield, P. F. *J. Phys. Chem. B* **2000**, *104*, 4815.

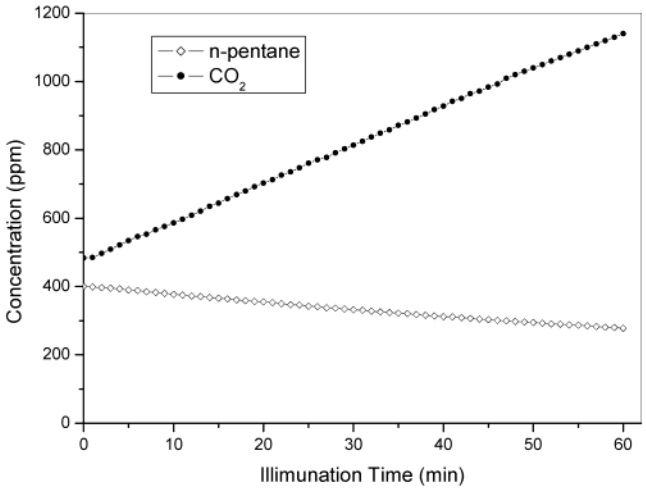

Figure 9. Concentration−time plots of *n*-pentane and CO_2 (degradation of *n*-pentane on the illuminated as-prepared SM-2).

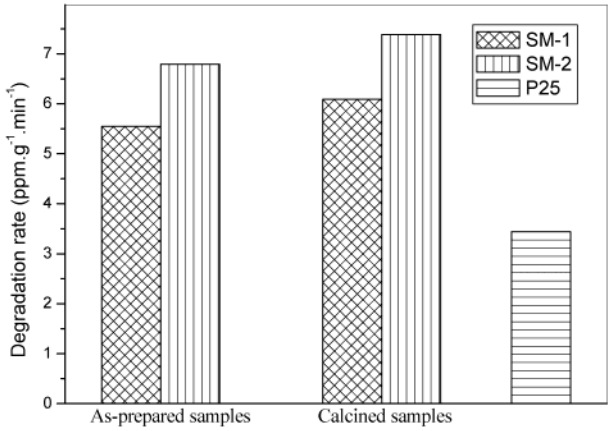

Figure 10. Photocatalytic activities of the as-prepared and calcined SM-1, SM-2, and P25.

tion of surfactant can all be accomplished in one step. As shown in Figure 8, SM-1 and SM-2 have more surface adsorbed water and hydroxyl groups than P25, possibly due to their larger surface areas.

Photocatalytic Activity on Oxidation of *n*-Pentane in Air. Photocatalytic activities of the as-prepared and calcined SM-1 and SM-2 are evaluated by using the oxidation of *n*-pentane in air. For comparison, the activity of commercial photocatalyst P25 was also tested under identical conditions. Figure 9 shows the concentration change of *n*-pentane and carbon dioxide with time on the illuminated as-prepared SM-2. It can be seen that the concentration of carbon dioxide produced was 5 times greater than the amount of *n*-pentane destroyed. It was also observed that the concentration of *n*-pentane and carbon dioxide changed linearly with increase in UV illumination time. Therefore, we concluded that *n*-pentane was decomposed completely. The *n*-pentane degradation rate constant (ppm·min^{-1}·g^{-1}, the average amount of *n*-pentane degraded per minute during the 60-min period per gram of the catalyst) was used to express the photocatalytic activity of TiO_2.

Examination of degradation rates of all photocatalysts in Figure 10 shows that the as-prepared SM-1 and SM-2 exhibit better photocatalytic activities than P25. Figure 10 also shows that the activities of SM-1 and SM-2 increase after calcination, with the calcined SM-2 having the highest photocatalytic activity. This can be attributed to the better crystallization of TiO_2 in SM-2, as demonstrated by the DTA curves.

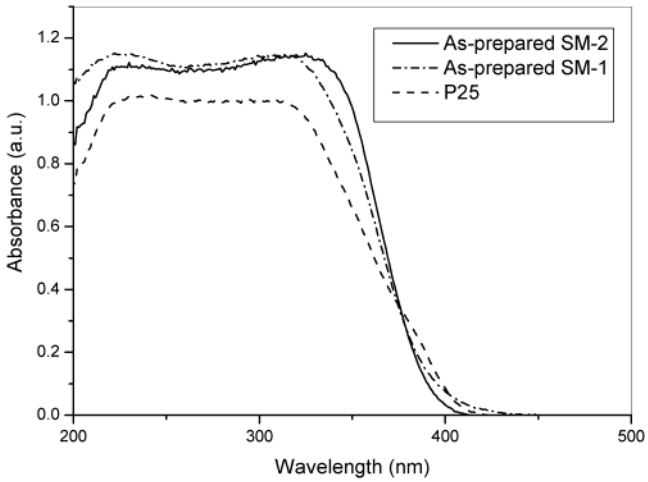

Figure 11. UV−Vis spectra of the as-prepared SM-1, SM-2, and P25.

The high activities of SM-1 and SM-2 can be attributed to the high brookite content. It has been reported that brookite TiO_2 powders of small crystallite size (<25 nm) exhibited high photocatalytic activity on redox reactions in aqueous 2-propanol and silver sulfate solution.[29] We have also demonstrated that a sonochemically prepared photocatalyst containing 20% brookite had better photocatalytic activity than a commercial photocatalyst with 20% rutile.[13] The electronic structure of brookite is similar to that of anatase because there are only minor differences in the local crystal environment between the two phases.[30] To the best of our knowledge, there is no reported experimental band gap data of brookite. However, calculation shows that the direct band gap of brookite is 0.42 and 0.16 eV larger than those of rutile and anatase, respectively.[30] Figure 11 shows the UV−vis absorbance spectra of the as-prepared SM-1, SM-2, and P25. The band gaps of the as-prepared SM-2, SM-1, and P25 are estimated to be 3.19, 3.16, and 3.08 eV from the $\alpha^{1/2}$ versus photon energy plots (Figure 12), respectively.[31] We believe that the larger band gap of our sample can be attributed to the quantum size effect and the existence of brookite. This is because the band gap of the as-prepared SM-2 containing more brookite is larger than that of the as-prepared SM-1, while the as-prepared SM-1 has smaller crystalline size than the as-prepared SM-2.

It is commonly accepted that a larger band gap corresponds to a more powerful redox ability. Because the photocatalytic process system can be considered similar to an electrochemical cell, the increase in band gap results in an enhanced oxidation−reduction potential based on the equation.

$$\Delta G = -ZEF \tag{4}$$

In eq 4, E represents the band gap of the semiconductor, ΔG is the free energy change of the redox process

(29) Ohtani, B.; Handa, J. I.; Nishimoto, S. I.; Kagiya, T. *Chem. Phys. Lett.* **1985**, *120*, 292.
(30) Mo, S. D.; Ching, W. Y. *Phys. Rev. B* **1995**, *51*, 13023.
(31) Tang, H.; Prasad, K.; Sanjinès, R.; Schmid, P. E.; Lévy, F. *J. Appl. Phys.* **1994**, *75*, 2042.

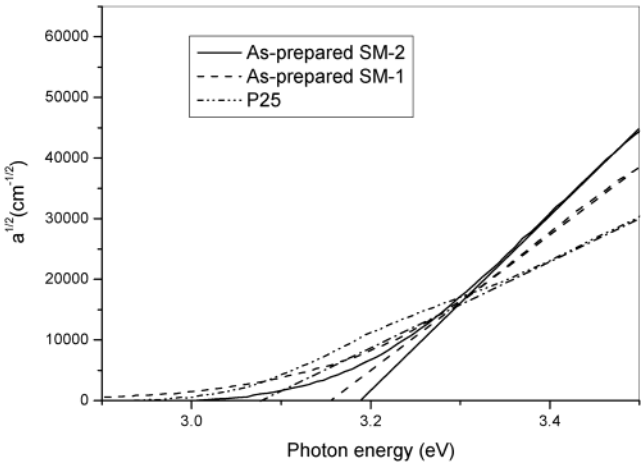

Figure 12. Plots of $\alpha^{1/2}$ versus photon energy for the as-prepared SM-1, SM-2, and P25; α is absorption coefficient.

occurring in the system, *Z* is a positive integer number equal to the number of elementary charges involved in the redox process, and *F* is the Faraday constant.[32] This indicates that brookite should be a more powerful photocatalyst than anatase. Furthermore, it is widely accepted that the high photocatalytic activity of P25 is partially due to its composite components consisting of 80% anatase and 20% rutile, which can inhibit the recombination of excited electron and hole pairs by modifying the electronic properties of TiO_2.[33,34] It can therefore be said that the composite materials of brookite and anatase can also suppress the recombination of electron and hole pairs similar to the couple materials of ZnO and TiO_2.[35]

The large surface area of SM-1 and SM-2 can adsorb significant amounts of water and hydroxyl groups. The surface adsorbed water and hydroxyl groups can react with photoexcited holes on the catalyst surface and produce hydroxyl radicals, which are powerful oxidants in degrading organics.[36] The large amounts of hydroxyl groups on the surface of SM-1 and SM-2 could also assist in stabilizing electron−hole pairs.[37] Although long range ordered M41S materials are desirable for electronic and photonic applications where structural periodicity is important, the interconnected mesoporous wormhole framework can promote diffusion of reactants and products, enhancing the activity by facilitating access to reactive sites of mesoporous TiO_2.[23,38]

Conclusions

Mesoporous TiO_2 with a bicrystalline (anatase and brookite) framework was synthesized directly under high-intensity ultrasound irradiation. This was carried out separately, both with and without the use of a triblock copolymer. Ultrasound irradiation was observed to assist the formation of brookite, but destroyed the ordered mesostructure in this case. As a result of using the triblock copolymer, the brookite content increased, along with the pore size and crystalline sizes of anatase and brookite. The hybrid inorganic/organic precursor formed between the triblock copolymer and titanium isopropoxide promoted the formation of brookite. It was also found that the as-prepared mesoporous TiO_2, containing anatase and brookite phases, had high photocatalytic activity. This was observed to increase even more after calcination because of better crystallization. The high photocatalytic activity of mesoporous TiO_2 with a bicrystalline framework can be attributed to the combined effect of three factors: high brookite content, high surface area, and the existence of mesopores. With ultrasound irradiation, the hydrolysis of titanium isopropoxide, crystallization of amorphous TiO_2, and extraction of the surfactant can all be accomplished in one step.

Acknowledgment. The work described in this paper was partially supported by a grant from the Research Grants Council of the Hong Kong Special Administrative Region, China (Project CUHK 4027/02P).

CM0203924

(32) Lin, J.; Yu, J. C.; Lo, D.; Lam, S. K. *J. Catal.* **1999**, *183*, 368.
(33) Bickley, R. I.; Gonzalez-Carreno, T.; Lees, J. S.; Palmisano, L.; Tilly, R. J. D. *J. Solid State Chem.* **1991**, *92*, 178.
(34) Fotou, G. P.; Pratsinis, S. *Chem. Eng. Commun.* **1996**, *151*, 251.
(35) Marci, G.; Augugliaro, V.; López-Muñoz, M. J.; Martín, C.; Palmisano, L.; Rives, V.; Schiavello, M.; Tilley, R. J. D.; Venezia, A. M. *J. Phys. Chem. B* **2001**, *105*, 1033.
(36) Turchi, C. S.; Ollis, D. F. *J. Catal.* **1990**, *122*, 178.
(37) Tsai, S. J.; Cheng, S. *Catal. Today* **1997**, *33*, 227.
(38) Shan, Z.; Gianotti, E.; Jansen, J. C.; Peters, J. A.; Marchese, L.; Maschmeyer, T. *Chem. Eur. J.* **2001**, *7*, 1437.